

**MIKE 21 Maritime**  
**Frequency Response Calculator and Mooring Analysis**  
Scientific Documentation



**DHI A/S headquarters**

Agern Allé 5  
DK-2970 Hørsholm  
Denmark

+45 4516 9200 Telephone

[mike@dhigroup.com](mailto:mike@dhigroup.com)

[www.mikepoweredbydhi.com](http://www.mikepoweredbydhi.com)

Company Registration No.: DK36466871

## PLEASE NOTE

### **COPYRIGHT**

This document refers to proprietary computer software, which is protected by copyright. All rights are reserved. Copying or other reproduction of this manual or the related programmes is prohibited without prior written consent of DHI A/S (hereinafter referred to as “DHI”). For details, please refer to your ‘DHI Software Licence Agreement’.

### **LIMITED LIABILITY**

The liability of DHI is limited as specified in Section III of your ‘DHI Software Licence Agreement’:

‘IN NO EVENT SHALL DHI OR ITS REPRESENTATIVES (AGENTS AND SUPPLIERS) BE LIABLE FOR ANY DAMAGES WHATSOEVER INCLUDING, WITHOUT LIMITATION, SPECIAL, INDIRECT, INCIDENTAL OR CONSEQUENTIAL DAMAGES OR DAMAGES FOR LOSS OF BUSINESS PROFITS OR SAVINGS, BUSINESS INTERRUPTION, LOSS OF BUSINESS INFORMATION OR OTHER PECUNIARY LOSS ARISING OUT OF THE USE OF OR THE INABILITY TO USE THIS DHI SOFTWARE PRODUCT, EVEN IF DHI HAS BEEN ADVISED OF THE POSSIBILITY OF SUCH DAMAGES. THIS LIMITATION SHALL APPLY TO CLAIMS OF PERSONAL INJURY TO THE EXTENT PERMITTED BY LAW. SOME COUNTRIES OR STATES DO NOT ALLOW THE EXCLUSION OR LIMITATION OF LIABILITY FOR CONSEQUENTIAL, SPECIAL, INDIRECT, INCIDENTAL DAMAGES AND, ACCORDINGLY, SOME PORTIONS OF THESE LIMITATIONS MAY NOT APPLY TO YOU. BY YOUR OPENING OF THIS SEALED PACKAGE OR INSTALLING OR USING THE SOFTWARE, YOU HAVE ACCEPTED THAT THE ABOVE LIMITATIONS OR THE MAXIMUM LEGALLY APPLICABLE SUBSET OF THESE LIMITATIONS APPLY TO YOUR PURCHASE OF THIS SOFTWARE.’

# CONTENTS

## MIKE 21 Maritime Frequency Response Calculator and Mooring Analysis Scientific Documentation

<b>1</b>	<b>Introduction .....</b>	<b>1</b>
<b>2</b>	<b>Application Areas.....</b>	<b>2</b>
<b>3</b>	<b>Basic Equations .....</b>	<b>3</b>
3.1	Geometry and motion of the floating body .....	3
3.1.1	Volume .....	4
3.1.2	Centre of buoyancy .....	4
3.2	Equation of motion .....	5
3.3	Added mass and damping coefficients $a_{jkt}$ and $K_{jkt}$ from radiation potential (1 <sup>st</sup> order) .....	6
3.3.1	Radiation potential.....	6
3.3.2	Boundary element method .....	7
3.3.3	Added mass and damping coefficients $A_{ij\omega}$ and $B_{ij\omega}$ in the frequency domain.....	8
3.3.4	Inverse transforms.....	8
3.3.5	Response amplitude operators .....	8
3.4	Wave drift forces (2 <sup>nd</sup> order).....	9
3.5	Wave exciting force $F_jDt$ .....	10
3.5.1	Linearization of the Boussinesq wave results .....	11
3.5.2	Inverse transforms.....	13
3.6	Hydrostatic and gravitational restoring coefficients $C_{jk}$ .....	13
3.7	Inertial coefficients $M_{jk}$ .....	14
3.8	External force $F_j, nlt$ .....	14
3.8.1	Viscous damping forces $F_j, visct$ .....	14
3.8.2	Mooring forces $F_j, moort$ .....	15
3.8.3	Wind forces .....	20
3.8.4	Current forces.....	21
<b>4</b>	<b>Numerical Implementation .....</b>	<b>22</b>
4.1	Implementation of the theory.....	22
4.2	Irregular frequencies .....	23
4.3	Convergence mode .....	24
<b>5</b>	<b>Output Data.....</b>	<b>25</b>
5.1	Frequency Response Calculator .....	25
5.1.1	Global output files.....	25
5.1.2	Vessel-specific output files.....	26
5.2	MIKE 21 MA .....	26
5.2.1	Global output files.....	26
5.2.2	Vessel-specific output files.....	27

<b>6</b>	<b>References.....</b>	<b>28</b>
6.1	Further reading on MIKE 21 MA and its predecessors .....	28
<b>A</b>	<b>The Haskind Relation.....</b>	<b>A-1</b>

# 1 Introduction

MIKE 21 Mooring Analysis (MA) is a dynamic mooring analysis software, which uses the vessel hull shape and associated gyrostatic data to derive the frequency response characteristics in the frequency domain and uses them to calculate the motions of the floating vessel under specific (static and/or dynamic) environmental conditions and in dependence of the mooring arrangement.

Flow, wave, and wind conditions can be provided as two-dimensional data, taking into account shear currents or complex wave fields, which are found in ports. Thereby, it takes advantage of the 2D results of the MIKE 21 Hydrodynamic (HD) module and the MIKE 21 Boussinesq Wave (BW) module.

It solves the equation of motion for the floating body in all six degrees of freedom and accounts for

- the exact three-dimensional vessel hull geometry and gyrostatic data
- bound and free long-period waves in shallow water
- frictional damping on the fenders in surge, heave, and roll modes
- viscous damping in surge and sway modes
- wind forces
- current forces
- 1<sup>st</sup> order wave forces
- 2<sup>nd</sup> order wave drift forces (assuming Newman's approximation)

This document presents the scientific background for the Mooring Analysis modelling system, which consists of the two maritime tools; Frequency Response Calculator (FRC) and MIKE 21 MA. Application areas are outlined in Section 2. The main equations are given in Section 3, followed by numerical aspects in Section 4. Finally, output data is specified in Section 5, followed by references and additional literature.

## 2 Application Areas

The MIKE 21 Maritime models Frequency Response Calculator (FRC) and MIKE 21 Mooring Analysis (MA) are used for the assessment of vessel motions and mooring forces under specific environmental conditions.

The model can be applied in

- Ports and terminals
- Harbours and marinas
- Offshore environments
  - Offshore moorings
  - Offshore tandem moorings
  - Floating wind turbines
  - Ships at anchor

The model can be used directly to evaluate mooring systems with respect to forces and vessel motions, e.g. to optimise port and offshore terminals, floating storage and production units, floating wind turbines, etc.

A major application area is the calculation of downtime/operability of a planned terminal. The situation is depicted in Figure 2-1.

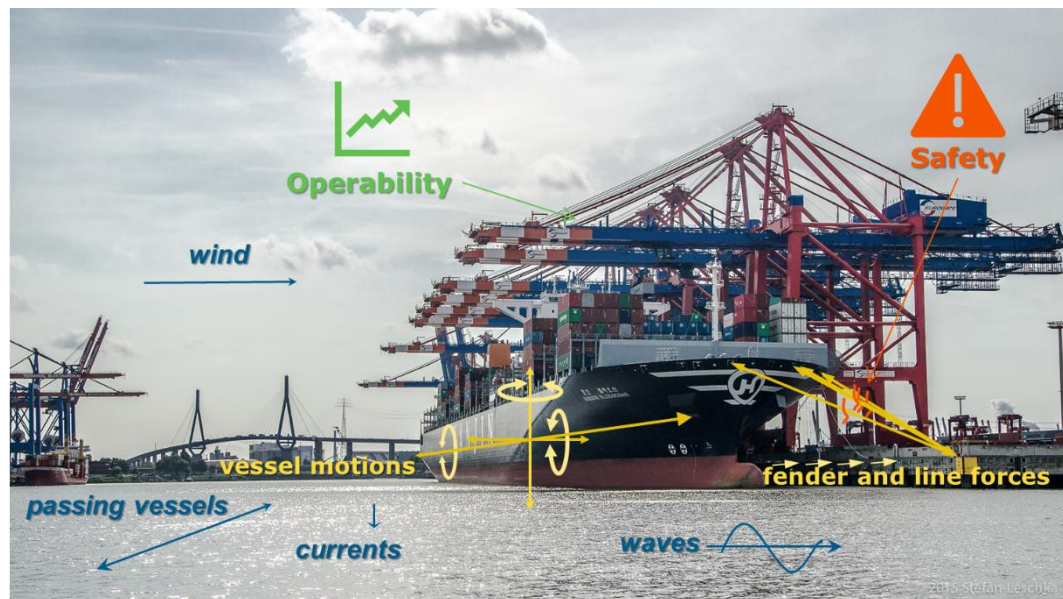


Figure 2-1 Illustration of a typical application area of MIKE 21 MA: vessel serviced at a terminal.

The moored vessel is subject to winds, currents, waves, and drawdown originating from passing vessels. They can be incorporated in the analyses as time series (e.g. derived from spectral information, dfs0 files) or as two-dimensional fields (e.g. derived using MIKE 21 HD or MIKE 21 BW, dfs2 files). The vessel motions and the forces in mooring lines, anchor chains, Trelleborg AutoMoor and fenders are calculated in MIKE 21 MA. The calculated motions are then to be compared with guidelines on critical motions to assess the terminal operability. The resulting mooring line forces can be related to maximum breaking loads to assess the safety for the investigated conditions.

### 3 Basic Equations

The solution of the hydrodynamic problem of a floating body subjected to environmental conditions such as ocean waves or passing vessels can be obtained by applying linear potential flow theory to the fluid domain. Thereby, surface waves are assumed to be regular (harmonic) waves of small amplitude. Applying linear boundary conditions on the fluid free-surface and body-surface is known as the Boundary Value Problem (BVP). Eventually, the computation of the velocity potential as the solution to the BVP allows derivation of the hydrodynamic coefficients and excitation forces caused by waves on the geometry surface (see /4/). The vessel motions are subsequently derived applying linear equations for floating body's response in regular waves. This process is illustrated in Figure 3-1.

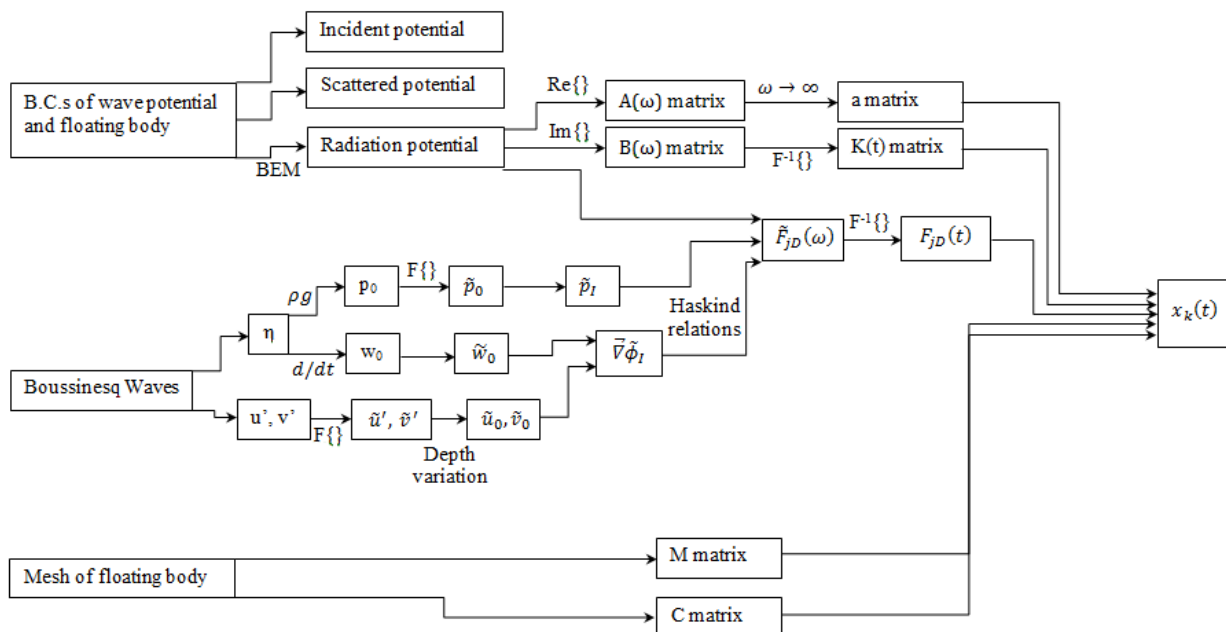


Figure 3-1 Flow chart of variables.

In this section, the geometrical conventions are defined in Section 3.1, followed by the equations of motion in time and frequency domain in Section 3.2, which are populated by coefficient matrices. Added mass and damping coefficients are derived from the radiation potentials, which are outlined in Section 3.3, followed by the 2<sup>nd</sup> order wave drift forces. The radiation potentials lead also to the formulation of the wave exciting forces, which is described in Section 3.5. They take further into consideration the linearized incident Boussinesq wave model data. Sections 3.6 and 3.7 state the hydrostatic and gravitational resorting coefficients and the inertial coefficients, respectively. In Section 3.8, the external forces originating from viscous damping, mooring, wind, and current are given.

#### 3.1 Geometry and motion of the floating body

For the floating body motions, the naval architect's convention is used, which is depicted in Figure 3-2.



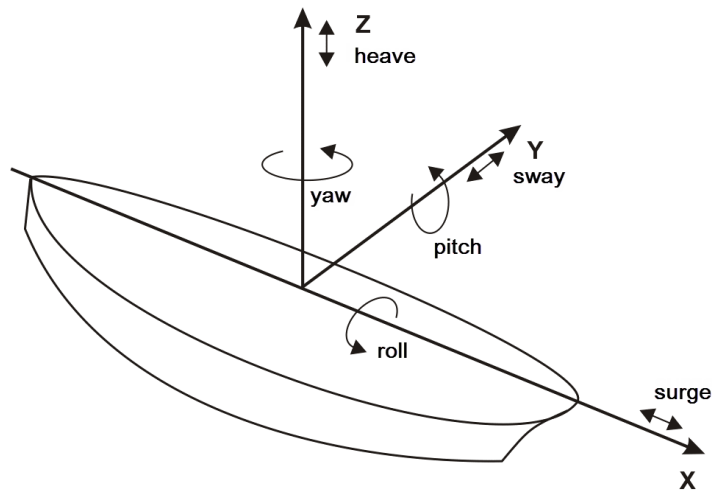


Figure 3-2 Definition of the six degrees of freedom of a floating body.

The six degrees of freedom are addressed using the unit normal vector  $n_j$  with

- $j = 1$ : translation along the  $x$  axis – surge
- $j = 2$ : translation along the  $y$  axis – sway
- $j = 3$ : translation along the  $z$  axis – heave
- $j = 4$ : rotation around the  $x$  axis – roll
- $j = 5$ : rotation around the  $y$  axis – pitch
- $j = 6$ : rotation around the  $z$  axis – yaw

In the following equations, the origin of the reference frame  $(0, 0, 0)$  is located in the longitudinal centre of gravity, the centreline and at the still water surface. The vertical axis is pointing positive upwards. The angle of attack of the environmental forcings  $\beta$  such as waves, is defined counter-clockwise with  $\beta = 0$  in positive direction of  $x$ .

The following sections define the volume of the floating body by the vessel hull surface and its coordinate of the centre of buoyancy.

### 3.1.1 Volume

The surfaces of the floating body  $S_b$  obtained from the vessel hull grid file are integrated in each of the three directions independently

$$V = - \iint_{S_b} n_1 x dS = - \iint_{S_b} n_2 y dS = - \iint_{S_b} n_3 z dS \quad (1)$$

where  $n_1$ ,  $n_2$  and  $n_3$  are the  $x$ ,  $y$  and  $z$  unit vectors normal to the body boundary and the median of the three volumes.

### 3.1.2 Centre of buoyancy

The position of the centre of buoyancy is required in the calculations of some of the components of the hydrostatic restoring matrix. Similarly, the surfaces obtained from the mesh are integrated accordingly with

$$x_b = \frac{-1}{2V} \iint_{S_b} n_1 x^2 dS \quad (2)$$

3

$$y_b = \frac{-1}{2V} \iint_{S_b} n_2 y^2 dS \quad (4)$$

$$z_b = \frac{-1}{2V} \iint_{S_b} n_3 z^2 dS \quad (5)$$

The centre of buoyancy  $(x_b, y_b, z_b)$  within the coordinate system shown in Figure 3-2 defines the space for the equation of motion outlined in the following section.

### 3.2 Equation of motion

The hydrodynamic interaction between the fluid and the floating body is assumed to be well described by linear potential flow theory. This approach is theoretically valid when

$$\frac{kA}{\tanh(kh)} \ll 1 \quad (6)$$

in which  $A$  is the wave amplitude,  $k$  is the wave number and  $h$  is the water depth. It is further assumed that the body motion remains small (ensured by the mooring system), and estimates for the neglected hydrodynamic effects can be included in the form of empirical coefficients /2/.

Under these assumptions, the equation of motion can be solved in the time domain and reads

$$\sum_{k=1}^6 (M_{jk} + a_{jk}) \ddot{x}_k(t) + \int_0^t K_{jk}(t - \tau) \dot{x}_k(\tau) d\tau + C_{jk} x_k(t) = F_{jD}(t) + F_{jnl}(t) \quad (7)$$

The first term at the left-hand side describes the inertia forces, the second term the hydrodynamic forces to first order in the body motion and the wave steepness and the third term the hydrostatic forces /2/. They are referred to as impulse-response functions (IRF's).

The matrices  $M_{jk}$ ,  $C_{jk}$  and  $K_{jk}$  are 6 x 6 matrices of the floating body system.  $M_{jk}$  and  $C_{jk}$  are the inertia restoring matrix and the hydrostatic restoring matrices, respectively.  $a_{jk}$  are impulsive (added mass) contributions, originating from the  $t = 0$  limit of the radiation problem. The forces due to radiated waves generated by the body's motions are expressed as a convolution of the radiation impulse response functions,  $K_{jk}$  /2/.

The right-hand side summarizes all non-linear external forces such as those from the mooring system and viscous and frictional damping (Froude-Krylov force),  $F_{jnl}(t)$ , and the wave exciting forces due to scattering of the incident waves,  $F_{jD}(t)$ .

The position and angular rotation of the body in six rigid-body degrees of freedom  $x_j(t)$  are expressed in Cartesian coordinates, where  $x_1 = x$  is aligned with the longitudinal ship axis pointing forward. The translations are indicated as  $x_1 =$  surge,  $x_2 =$  sway and  $x_3 =$  heave. The rotational motions are  $x_4 =$  roll angle,  $x_5 =$  pitch angle and  $x_6 =$  yaw angle (refer to Figure 3-2). The over-dot indicates differentiation with respect to time  $t/2$ .

The second term in equation (7) makes deriving of the matrices  $K_{jk}(t)$ ,  $a_{jk}(t)$  inefficient in the time domain due to the convolution with time  $t$ . Therefore, the hydrodynamic calculations are performed in the frequency domain.

For deriving the hydrodynamic coefficients in the frequency domain, the equivalent of the time-domain impulse response functions (IRF's) is used. In the context of linear potential flow theory, this equivalent is obtained by taking the incident wave to be time-harmonic with the wave frequency,  $\omega$ , and complex amplitude,  $\tilde{\zeta}$ . This leads to the frequency response functions

$$\sum_{k=1}^6 \left\{ -\omega^2 [M_{jk} + A_{jk}(\omega)] + i\omega B_{jk}(\omega) + C_{jk} \right\} \tilde{x}_k(\omega) = \tilde{F}_{jD}(\omega), \quad j = 1, 2, \dots, 6 \quad (8)$$

for the hydrodynamic coefficient matrices added mass  $A_{jk}(\omega)$ , damping  $B_{jk}(\omega)$ , hydrostatic and gravitational restoring coefficients  $C_{jk}$ , and exciting forces  $\tilde{F}_{jD}(\omega)$ .

### 3.3 Added mass and damping coefficients $a_{jk}(t)$ and $K_{jk}(t)$ from radiation potential (1<sup>st</sup> order)

#### 3.3.1 Radiation potential

Even though part of the surface elevation and flow field is solved by Boussinesq waves in MIKE 21 MA, integral equations for the flow potential need to be solved to obtain the potential for radiated waves. This is done in the frequency domain.

The total wave potential can be decomposed into incident ( $j = 0$ ), scattered ( $j = 7$ ) and radiated wave modes ( $j = 1, 2, \dots, 6$ ) respectively

$$\varphi = \varphi_0 + \varphi_7 + i\omega \sum_{j=1}^6 \xi_j \varphi_j \quad (9)$$

$\xi_j$  refers to the six degree of freedom response of the floating body, thus  $\varphi_j$  has a different unit compared to the other two components. It can be understood as the wave potential per unit velocity of the floating body.

The velocity potential for the incident waves is defined as

$$\varphi_0 = \frac{igA \cosh [k(z+h)]}{\omega \cosh(kh)} e^{-i(kxcos\beta - kysin\beta)} \quad (10)$$

with the coordinates  $(x, y, z)$ . Note that  $z$  is related to the water surface.

On the surface of the floating body, the condition in the expression

$$\frac{\partial \varphi_7}{\partial n} = -\frac{\partial \varphi_0}{\partial n} \quad (11)$$

has to be satisfied. For all eight modes  $j = \{0,1, \dots, 7\}$ , the linearized form of the surface boundary condition is implemented at the surface, where  $z = 0$  as shown in the equation

$$-\frac{\omega^2}{g} \varphi_j + \frac{\partial \varphi_j}{\partial z} = 0 \quad (12)$$

Using the boundary conditions, the Laplacian of the wave potential has to be solved for all 8 modes (where  $j = \{0,1,2, \dots, 7\}$ ); one each for incident and scattered, and six for each degree of freedom of the radiated waves

$$\nabla^2 \varphi_j = 0 \quad (13)$$

### 3.3.2 Boundary element method

The frequency boundary value problems governed by the Laplace equation (13) are solved to obtain the radiation potential  $\varphi_j$  on the surface of the floating body

$$\frac{\partial \varphi_j(x_i)}{\partial n} = n(x_i) \quad (14)$$

with the normal velocity for each mode  $n$ . When written on the control point of each panel of the body, the integral equations of the boundary element method are transformed into a linear system of equations

$$\frac{\sigma_R(x_i)}{2} + \sum_{k=1}^N \sigma_R(x_k) K_{ik} = \frac{\partial \varphi_j(x_i)}{\partial n} \quad (15)$$

The integral equations use a source distribution in order to solve the source strengths  $\sigma_R$  by calculating the radiation impulse response functions in the  $N \times N$  matrix

$$K_{ik} = -\frac{1}{4\pi} \frac{\partial}{\partial N_{x_i}} \iint_S G(x_i; x_k) dS(x_k) \quad (16)$$

In this equation,  $G(x_i; x_k)$  is the free-surface Green's function with  $x_i$  and  $x_k$ , which are the field and source points, respectively [1].

The radiation potential can then be derived using

$$\varphi_j(x_i) = -\sum_{k=1}^N \sigma_R(x_k) S_{ik} \quad (17)$$

where

$$S_{ik} = \frac{1}{4\pi} \iint_S G(x_i; x_k) dS(x_k) \quad (18)$$

### 3.3.3 Added mass and damping coefficients $A_{ij}(\omega)$ and $B_{ij}(\omega)$ in the frequency domain

The added mass and damping coefficient matrices are obtained from the radiation potentials  $\varphi_j^R$  as defined by

$$A_{ij} - \frac{i}{\omega} B_{ij} = \rho g \iint_{S_b} n_i \varphi_j^R dS \quad (19)$$

The real and imaginary part of this equation can be expressed by

$$A_{ij}(\omega) = \text{Re} \left\{ \rho \iint_{S_b} \varphi_j^R n_i dS \right\} \quad (20)$$

and

$$B_{ij}(\omega) = \text{Im} \left\{ \rho \iint_{S_b} \varphi_j^R n_i dS \right\} \quad (21)$$

### 3.3.4 Inverse transforms

Once  $A_{jk}$  is obtained, the added mass coefficients  $a_{jk}$  can be calculated from

$$A_{jk}(\omega) = a_{jk} - \frac{1}{\omega} \int_0^{\infty} K_{jk}(t) \sin \omega t dt \quad (22)$$

as  $\omega \rightarrow \infty$ , the second term vanishes. To obtain the damping coefficients, an inverse transform of  $K_{jk}(t)$  is required as shown in

$$B_{jk}(\omega) = \int_0^{\infty} K_{jk}(t) \cos \omega t dt \quad (23)$$

(see /5/).

### 3.3.5 Response amplitude operators

The response amplitude operators (RAO) are not directly provided. They are obtained by equation

$$\sum_{j=1}^6 \xi_j [-\omega^2 (M_{ij} + a_{ij}) + i\omega b_{ij} + c_{ij}] = AX_i \quad (24)$$

where  $\omega$  is the angular wave frequency,  $\xi_j$  is the body motion,  $a_{ij}$ ,  $b_{ij}$  and  $c_{ij}$  are added mass, damping and restoring matrices, respectively.  $X_i$  is the wave excitation force per unit wave amplitude, and  $A$  is the wave amplitude.

The equation is solved for the body motion  $\xi_j$ , and the complex RAO for the  $j$ th mode is obtained by

$$Z_j(\omega, \theta) = \frac{\xi_j}{A} = \sum_{i=1}^6 [C_{ij}]^{-1} X_i \quad (25)$$

where  $[C_{ij}]^{-1}$  indicates the inverse matrix of the member between the brackets in the equation of motion. The RAO are given for each angular wave frequency  $\omega$  and incident wave direction  $\theta$  /10/.

$$A = A^{(1)} \cos(\omega t) + A^{(2)} \sin(\omega t) = \Re(\tilde{A} e^{-i\omega t}) \quad (26)$$

where  $\tilde{A} = A^{(1)} + iA^{(2)}$ . The imaginary part of the harmonic motion is defined as phase lag relative to the real component /10/.

### 3.4 Wave drift forces (2<sup>nd</sup> order)

Second order wave drift forces apply the Newman's approximation /8/ and are derived by solving the source distribution for the diffraction problem,  $\sigma_D$ , in each incident wave direction  $\beta$

$$\frac{\sigma_D(x_i)}{2} + \sum_{k=1}^N \sigma_D(x_k) K_{ik} = -\frac{\partial \varphi_0(x_i)}{\partial n} \quad (27)$$

In the frequency domain, the second order drift forces are computed by the far field formula /13/. The mean surge and sway forces

$$F \begin{pmatrix} x \\ y \end{pmatrix} (\beta) = -2\pi\rho \frac{k * (k_{inf} * h)^2}{h \left( (k * h)^2 - (k_{inf} * h)^2 + k_{inf} * h \right)} * \int_0^{2\pi} |H(\theta)|^2 * \begin{pmatrix} \cos(\theta) \\ \sin(\theta) \end{pmatrix} d\theta - 2\pi\rho\omega * \begin{pmatrix} \cos(\beta) \\ \sin(\beta) \end{pmatrix} * Im(H(\beta)) \quad (28)$$

with the wave propagation direction  $\beta$ , the water density  $\rho$ , the wave number  $k$ , the water depth  $h$ , the incident wave direction  $\theta$ , the infinite depth wave number  $k_{inf}$ , and the Kochin function  $H$  from 0 to  $2\pi$  /5/.

The mean yaw moment

$$M_z(\beta) = 2\pi * \frac{\rho\omega}{k} * Re(H'(\beta)) - \frac{2\pi\rho(k_{inf} * h)^2}{h \left( (k * h)^2 - (k_{inf} * h)^2 + k_{inf} * h \right)} * Im \left( \int_0^{2\pi} \overline{H(\theta)} * H'(\theta) d\theta \right) \quad (29)$$

where  $H$  is the Kochin function. It is defined as

$$H(\theta) = H_D(\theta) * e^{i*\frac{\pi}{2}} + i\omega * \sum_{i=1}^6 Z_j * H_{R_j}(\theta) e^{-i*\frac{\pi}{2}} \quad (30)$$

where  $H_D$  and  $H_R$  are the diffraction and radiation contributions to the Kochin function, and  $Z_j$  is the response amplitude operator (see Section 3.3.5). For the radiated wave modes ( $j = 1, 2, \dots, 6$ ),

$$\varphi_j(r, \theta, z) = \frac{\cosh(k(z+h))}{\cosh(kh)} * \sqrt{\frac{k}{2\pi r}} e^{i(kr - \frac{\pi}{4})} H_R(\theta) \quad (31)$$

For the scattered (diffraction) mode,

$$\varphi_7(r, \theta, z) = \frac{\cosh(k(z+h))}{\cosh(kh)} * \sqrt{\frac{k}{2\pi r}} e^{i(kr - \frac{\pi}{4})} H_D(\theta) \quad (32)$$

In the time domain, the drift force time series are computed by the method described in /14/.

It is noted that the assumption of the Newman's approximation due to the far-field solution effectively means that only the diagonal terms in the quadratic transfer function (QTF) are considered corresponding to the monochromatic frequency pairs. This only gives the mean drift force, and second order effects that are not described by the mean drift force are not included. This approximation is theoretically valid in deep water conditions, while in shallow water the full QTF matrix with the off-diagonal terms (bi-chromatic frequency pairs) should be considered. This is currently not implemented in MIKE 21 MA.

### 3.5 Wave exciting force $F_{jD}(t)$

The wave exciting force is expressed in terms of incident wave quantities and solutions to the radiation problem by means of the Haskind relations /11/

$$F_{jD}(t) = \iint_{S_b} p_I(\vec{x}, t) n_j(\vec{x}) d\vec{x} + \rho \int_{-\infty}^{\infty} \iint_{S_b} \dot{\phi}_{In}(\vec{x}, \tau) \phi_j(\vec{x}, t - \tau) d\vec{x} d\tau \quad (33)$$

(see also Appendix A). In this equation,  $\phi_I$  is a known incident wave potential, which satisfies the linear free-surface body condition and induces a first order dynamic pressure

$$p_I = \frac{\partial \phi_I}{\partial t} \quad (34)$$

in the fluid. The incident wave refers to the wave undisturbed by the presence of the body. A subscript  $n$  is used to indicate the operation  $\vec{n} \cdot \vec{\nabla}$ , with  $\vec{n}$  being the normal vector to the equilibrium wetted body surface  $S_b$ , while  $n_j$  is the generalized unit normal in six degrees of freedom.  $\phi_j$  is the solution to the  $j$ th mode impulse velocity radiation problem, which is defined by the boundary condition

$$\vec{n} \cdot \vec{\nabla} \phi_j = n_j \delta(t), \vec{x} \in S_b \quad (35)$$

with the Dirac function  $\delta(t)$ . The first term in equation (33) refers to the Froude-Krylov force, while the second term describes the scattering of the incident wave by the body when fixed to its equilibrium position /2/.

The scattering of the incident waves depends on the radiation potential of the floating body. This potential is derived in the frequency domain for linear incident waves (see Section 3.3). It is further related to the Boussinesq wave field, which is linearized and transferred to the frequency domain. This is explained in the following sections.

### 3.5.1 Linearization of the Boussinesq wave results

The results of a Boussinesq wave simulation have to be linearized to provide incident wave quantities required by the Haskind relations (see Section 3.5), to obtain the terms  $\tilde{p}_I(\vec{x}, \omega)$  and  $\tilde{\phi}_{In}(\vec{x}, \omega)$  to be used in equation (51).

Using the results from the free surface elevation  $\eta(\vec{x}, \omega)$  and depth-averaged velocities  $u'(\vec{x}, t)$  and  $v'(\vec{x}, t)$  from the Boussinesq model on a set of points on the intersection of the still water plane with the floating body  $\vec{x}$ , the depth-averaged velocity with depth variation  $z$  can be expressed as

$$u' = \frac{1}{D + \eta} \int_{-D}^{\eta} u(\vec{x}, z, t) dz \quad (36)$$

and

$$v' = \frac{1}{D + \eta} \int_{-D}^{\eta} v(\vec{x}, z, t) dz \quad (37)$$

In these equations,  $D$  is the draft of the vessel,  $z$  is the vertical coordinate pointing upwards, with  $z = 0$  at the water surface, and  $\eta$  is the water surface elevation /2/.

Based on the free surface elevation  $\eta(\vec{x}, t)$  from the Boussinesq model, the dynamic pressure

$$p_0(\vec{x}, t) = \rho g \eta(\vec{x}, t) \quad (38)$$

and the vertical velocity component

$$w_0(\vec{x}, t) = \dot{\eta}(\vec{x}, t) \quad (39)$$

are obtained using the linear free-surface boundary conditions. The subscript 0 indicates the variables at the free surface /2/.

These quantities in time domain  $p_0, u', v'$  and  $w_0$  have to undergo Fourier transformation to obtain the corresponding quantities as a function of the wave frequency

$$\tilde{F}_{jD}(\omega) = \int_0^{\infty} F_{jD}(t) e^{-i\omega t} dt \quad (40)$$

This transformation results in a series of sine and cosine functions

$$f_n = a_n \cos(nx) + b_n \sin(nx) \quad (41)$$

From linear wave theory, the velocity can be derived using



$$u = \frac{H g T}{2 L} \cos\theta \frac{\cosh[k(z+h)]}{\cosh(kh)} \quad (42)$$

The hyperbolic cosine terms are used in the equations

$$p(\vec{x}, z, t) = F^{-1} \left\{ \tilde{p}_0(\vec{x}, \omega) \frac{\cosh[k(z+h)]}{\cosh(kh)} \right\} \quad (43)$$

$$u'(\vec{x}, t) = F^{-1} \left\{ \tilde{u}'(\vec{x}, \omega) \frac{\cosh[k(z+h)]}{\cosh(kh)} \right\} \quad (44)$$

$$v'(\vec{x}, t) = F^{-1} \left\{ \tilde{v}'(\vec{x}, \omega) \frac{\cosh[k(z+h)]}{\cosh(kh)} \right\} \quad (45)$$

and

$$w(\vec{x}, z, t) = F^{-1} \left\{ \tilde{w}_0(\vec{x}, \omega) \frac{\sinh[k(z+h)]}{\sinh(kh)} \right\} \quad (46)$$

to include the hyperbolic depth variations. The linear dispersion relation

$$\omega^2 = gk \tanh(kh) \quad (47)$$

is utilized to determine the wave number  $k$ . It should further be noted that equations (44) and (45) apply the depth-averaged velocities directly, translating them directly to the frequency domain, denoted as  $\tilde{u}'$  and  $\tilde{v}'$ . They are used to derive the velocity at the intersection point between the structure and the still water surface. The relation is given in the equations (36) and (37). They can be rewritten as

$$\tilde{u}_0(\vec{x}, \omega) = \left\{ \tilde{u}'(\vec{x}, \omega) \frac{kh}{\tanh(kh)} \right\} \quad (48)$$

$$\tilde{v}_0(\vec{x}, \omega) = \left\{ \tilde{v}'(\vec{x}, \omega) \frac{kh}{\tanh(kh)} \right\} \quad (49)$$

The term  $\frac{kh}{\tanh(kh)}$  approaches unity in shallow water due to no variations in depth, and  $kh$  in deep waters /2/.

The quantity  $\tilde{p}_0$  is the incident pressure acting on the wetted body surface  $\tilde{p}_I$ . The normal derivative of the incident velocity potential  $\tilde{\phi}_I(\vec{x}, \omega)$  can be calculated from the velocities obtained in the three directions with equations (46), (48) and (49) /2/.

The sequence of quantities in this section is shown in the following expression.

$$\eta, u', v' \xrightarrow[\text{Free surface B.C.}]{\text{Free surface B.C.}} p_0, u', v', w_0 \xrightarrow[\text{Fourier transform}]{\text{Fourier transform}} \tilde{p}_0, \tilde{u}', \tilde{v}', \tilde{w}_0 \xrightarrow[\text{Depth variation}]{\text{Depth variation}} \tilde{p}_0, \tilde{u}_0, \tilde{v}_0, \tilde{w}_0 \quad (50)$$

### 3.5.2 Inverse transforms

Similar to the derivation of  $K_{jk}(t)$ , the exciting force  $F_{jD}(t)$  is obtained from the inverse transformation of  $\tilde{F}_{jD}(\omega)$ . It can then be expressed in terms of radiation potentials via the Haskind relation

$$\begin{aligned}\tilde{F}_{jD}(\omega) &= \int_0^{\infty} F_{jD}(t) e^{-i\omega t} dt \\ &= \iint_{S_b} \tilde{p}_I(\vec{x}, \omega) n_j(\vec{x}) d\vec{x} + i\omega\rho \iint_{S_b} \tilde{\phi}_j(\vec{x}, \omega) \tilde{\phi}_{In}(\vec{x}, \omega) d\vec{x}\end{aligned}\quad (51)$$

(see also Appendix A). The input terms  $\tilde{p}_I(\vec{x}, \omega)$  and  $\tilde{\phi}_{In}(\vec{x}, \omega)$  for the Haskind relation are derived from the Boussinesq wave field, e.g. calculated using MIKE 21 Boussinesq wave model results (MIKE 21 BW) as described in Section 3.5.1.

### 3.6 Hydrostatic and gravitational restoring coefficients $C_{jk}$

The hydrostatic and gravitational restoring matrix is independent of the wave frequency  $\omega$  and only depends on the geometry of the floating body. The matrix in the time domain  $C_{jk}(t)$  is expressed for the six degrees of freedom (see Figure 3-2) using the relations

$$\begin{aligned}C_{3,3}(t) &= \rho g \iint_{S_b} n_3 dS \\ C_{3,4}(t) &= C_{4,3}(t) = \rho g \iint_{S_b} y n_3 dS \\ C_{3,5}(t) &= C_{5,3}(t) = -\rho g \iint_{S_b} x n_3 dS \\ C_{4,4}(t) &= \rho g \iint_{S_b} y^2 n_3 dS + \rho g \forall z_b - mgz_g \\ C_{4,5}(t) &= C_{5,4}(t) = -\rho g \iint_{S_b} x y n_3 dS \\ C_{4,6}(t) &= -\rho g \forall x_b + mgx_g \\ C_{5,5}(t) &= \rho g \iint_{S_b} x^2 n_3 dS + \rho g \forall z_b - mgz_g \\ C_{5,6}(t) &= -\rho g \forall y_b + mgy_g\end{aligned}\quad (52)$$

The remaining coefficients of the unstated matrix are set to 0. Indices  $b$  and  $g$  denote the centre of buoyancy and the centre of gravity, respectively.  $\rho$  is the density of water,  $g$  is the gravitational acceleration,  $m$  is the mass and  $\forall$  is the volume,  $S$  indicates the surface of the floating body, and  $n_j$  is the normal vector of mode  $j$  /5/.

### 3.7 Inertial coefficients $M_{jk}$

The inertial coefficient matrix  $M_{jk}$  is set up under the assumption of free stable floatation with no external constraints. The mass is expressed as

$$m = \rho V$$

$$x_b = x_g, \quad y_b = y_g$$

$$M = \begin{bmatrix} m & 0 & 0 & 0 & mz_g & -my_g \\ 0 & m & 0 & -mz_g & 0 & mx_g \\ 0 & 0 & m & my_g & -mx_g & 0 \\ 0 & -mz_g & my_g & I_{11} & I_{12} & I_{13} \\ mz_g & 0 & -mx_g & I_{21} & I_{22} & I_{23} \\ -my_g & mx_g & 0 & I_{31} & I_{32} & I_{33} \end{bmatrix} \quad (53)$$

and the horizontal centre of gravity coordinates, denoted with index  $g$ , are set as the centre of buoyancy, denoted with index  $b$  (see Section 3.1.2). The vertical location of the centre of gravity depends on the weight distribution of the floating body (usually a ship), and largely depends on whether it is loaded or unloaded.

The moments of inertia

$$I_{ij} = \rho V r_{ij} |r_{ij}| \quad (54)$$

are obtained from the radii of gyration. The radii of gyration input consist of a (3x3) array of values of  $r / 5$ .

### 3.8 External force $F_{j,nl}(t)$

The total external force

$$F_{j,nl}(t) = F_{j,moor}(t) + F_{j,visc}(t) + F_{j,w}(t) + F_{j,c}(t) + F_{j,drift}(t) \quad (55)$$

is the sum of the mooring forces  $F_{j,moor}(t)$ , viscous damping forces  $F_{j,visc}(t)$ , wind forces  $F_{j,wind}(t)$ , current forces  $F_{j,cur}(t)$ , slow wave drift forces  $F_{j,drift}(t)$  and frictional damping forces  $F_{j,fric}(t)$  in the mooring system in each degree of freedom  $j$ . They are described in this section.

#### 3.8.1 Viscous damping forces $F_{j,visc}(t)$

The viscous damping force is defined as

$$F_{j,visc}(t) = B_j^0 + \sum_{k=1}^6 [B_{jk}^1 \dot{x}_k(t) + B_{jk}^2 \dot{x}_k(t) |\dot{x}_k(t)| + B_{jk}^3 \dot{x}_k^3(t)] \quad (56)$$

in which  $B^0$ ,  $B^1$ ,  $B^2$  and  $B^3$  are the constant, linear, quadratic and cubic damping coefficient matrices.  $\dot{x}_k(t)$  is the speed of motion into direction  $k$ .

### 3.8.2 Mooring forces $F_{j,moor}(t)$

#### Mooring lines

Given that the displacement of a floating body is expressed as

$$dl = l - l_0 \quad (57)$$

with the line length  $l$  and the unstretched line length  $l_0$ , then the elongation is proportional to the force in the mooring line  $dl \sim F_{j,moor,line}(t)$ . This relation is provided by means of a Load-excursion curve denoted as  $R(dl)$ ,

$$F_{j,line}(t) = R(dl) + F_{j,line,damp}(t) \quad (58)$$

which is line-material specific and which is provided as input data. From this relation, the mooring line force is calculated.  $F_{j,line,damp}(t)$  is a damping force, which can be applied for the purpose of calibration. It is governed by linear and quadratic damping coefficients  $B^1$  and  $B^2$  as part of the input data. It is derived with the relation

$$F_{j,line,damp}(t) = \sum_{k=1}^6 [B_{jk}^1 \dot{x}_k(t) + B_{jk}^2 \dot{x}_k(t) |\dot{x}_k(t)|] \cdot \text{line direction}_j(t) \quad (59)$$

where  $\dot{x}_k(t)$  is the speed of motion into direction  $k$ .  $\text{line direction}_j(t)$  is a vector pointing into the direction of the line.

#### Bollards

The line force vectors pointing from a bollard in the line direction  $\text{line direction}_j(t)$  and the bollard force and its components are depicted in Figure 3-3.

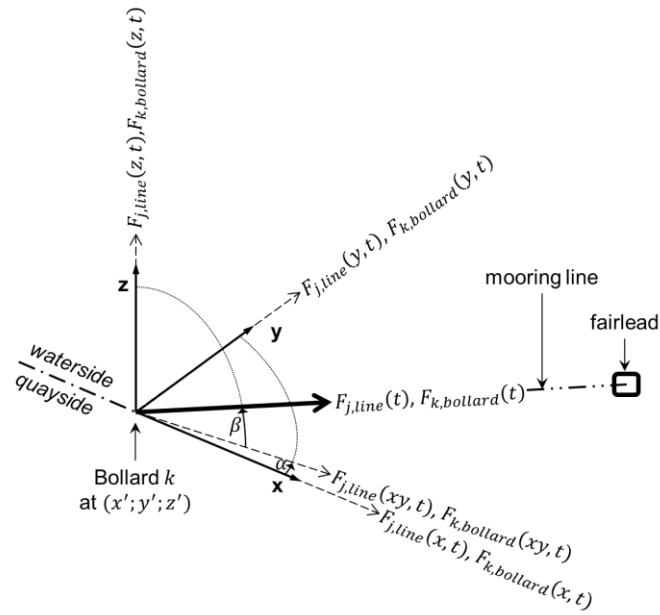


Figure 3-3. Principle sketch of bollard force and mooring line force components acting on a bollard.

The total bollard force  $F_{k,bollard}(t)$  on each bollard  $k$  are composed from its directional components

$$F_{k,bollard}(t) = \sqrt{F_{k,bollard}(x,t)^2 + F_{k,bollard}(y,t)^2 + F_{k,bollard}(z,t)^2} \quad (60)$$

The bollard force components are derived from the directional force components of each line  $j$  of the  $n$  lines attached to the bollard as given in equations (61) to (63)

$$F_{k,bollard}(x,t) = \sum_{j=1}^n F_{j,line}(x,t) \quad (61)$$

$$F_{k,bollard}(y,t) = \sum_{j=1}^n F_{j,line}(y,t) \quad (62)$$

$$F_{k,bollard}(z,t) = \sum_{j=1}^n F_{j,line}(z,t) \quad (63)$$

The force components in the horizontal dimensions  $x$  and  $y$  form the horizontal bollard force

$$F_{k,bollard}(xy,t) = \sqrt{F_{k,bollard}(x,t)^2 + F_{k,bollard}(y,t)^2} \quad (64)$$

while  $F_{k,bollard}(z,t)$  is the vertical bollard force.

The line forces components used in equations (65) to (68) are derived from the total mooring line force of each line  $j$  as follows:

$$F_{j,moor,line}(xy, t) = F_{j,moor,line}(t) \cos\beta \quad (65)$$

$$F_{j,moor,line}(x, t) = F_{j,moor,line}(xy, t) \cos\alpha \quad (66)$$

$$F_{j,moor,line}(y, t) = F_{j,moor,line}(xy, t) \sin\alpha \quad (67)$$

$$F_{j,moor,line}(z, t) = F_{j,moor,line}(t) \sin\beta \quad (68)$$

## Fenders

If the fender attachment point moves along the fender force direction with a displacement  $dl$ , then the fender is compressed by the same length. The fender compression is related to the fender force  $dl \sim F_n(t)$  by means of the fender deflection-reaction curve

$$F_{j,n}(t) = R(dl) + F_{j,fender,damp}(t) \quad (69)$$

which is fender-specific and which is provided as input data. The fender damping force

$$F_{j,fender,damp}(t) = \sum_{k=1}^6 B_{jk}^1 \dot{x}_k(t) \cdot \text{fender force direction}_j(t) \quad (70)$$

in which  $\dot{x}_k(t)$  is the speed of motion into direction  $k$  and  $B^1$  is the linear damping coefficient.  $\text{fender force direction}_j(t)$  is a vector pointing into the direction of the fender force.

Furthermore, the fender friction is calculated by

$$F_{j,fric}(t) = \mu F_{j,n}(t) \cdot \frac{vel_j(t)}{|vel(t)|} \quad (71)$$

with the fender friction coefficient  $\mu$  and the relative velocity between ship attachment point and fender attachment point  $vel(t)$ . The fender force then reads

$$F_{j,moor,fender}(t) = F_{j,n}(t) + F_{j,fric}(t) \quad (72)$$

## Trelleborg AutoMoor

A Trelleborg AutoMoor® (AM) is extended between a fixed point on the berth and a moving point on the vessel's hull. These points are shown in Figure 3-4. In this figure the support point on the berth, shown as (0, 0, 0), and the attachment point on the vessel's hull is (0, Y, 0). The AM coordinates are defined as Y in the initial AM arm direction, X the lateral (surge) displacement and Z the vertical (heave) displacement. Due to the vessel motions, X, Y and Z values vary by time and at each time step the AM forces applied to the vessel are interpolated from an input AM reaction force table. To interpolate the AM

forces at each time step, the values of  $\theta_x$ ,  $Y$  and  $\theta_z$  are needed in which  $\theta_x = ATAN(X/Y)$  and  $\theta_z = ATAN(Z/Y)$ . Different AM force components are then interpolated via the input force table,

$$F_{j,Interpolated}(t) = f(\theta_x, Y, \theta_z) \quad (73)$$

The AM force tables are provided for different initial AM length and maximum AM forces. There are 5 tables provided which include  $F_x$ ,  $F_y$ ,  $F_z$ ,  $F_{x\_restoring}$  and  $F_{y\_restoring}$ , where  $F_x$ ,  $F_y$ , and  $F_z$  are the components of a linear spring which works only under tension,  $F_{x\_restoring}$  and  $F_{y\_restoring}$  are the force components of a torsional spring in  $X$  and  $Y$  directions.

$$\begin{aligned} F_{x_{j,AM}} &= F_{x_{j,interpolated}} + F_{x_{restoring_{j,interpolated}}} \\ F_{y_{j,AM}} &= F_{y_{j,interpolated}} + F_{y_{restoring_{j,interpolated}}} \\ F_{z_{j,AM}} &= F_{z_{j,interpolated}} \end{aligned} \quad (74)$$

The mooring force applied to the vessel due to AutoMoor is

$$F_{j, moor, AM}(t) = F_{x_{j,AM}} \cdot e_{x, j} + F_{y_{j,AM}} \cdot e_{y, j} + F_{z_{j,AM}} \cdot e_{z, j} \quad (75)$$

Where,  $e_x$ ,  $e_y$ ,  $e_z$  are the unit vectors of the local  $x$ ,  $y$  and  $z$  directions with respect to the vessel coordinates.

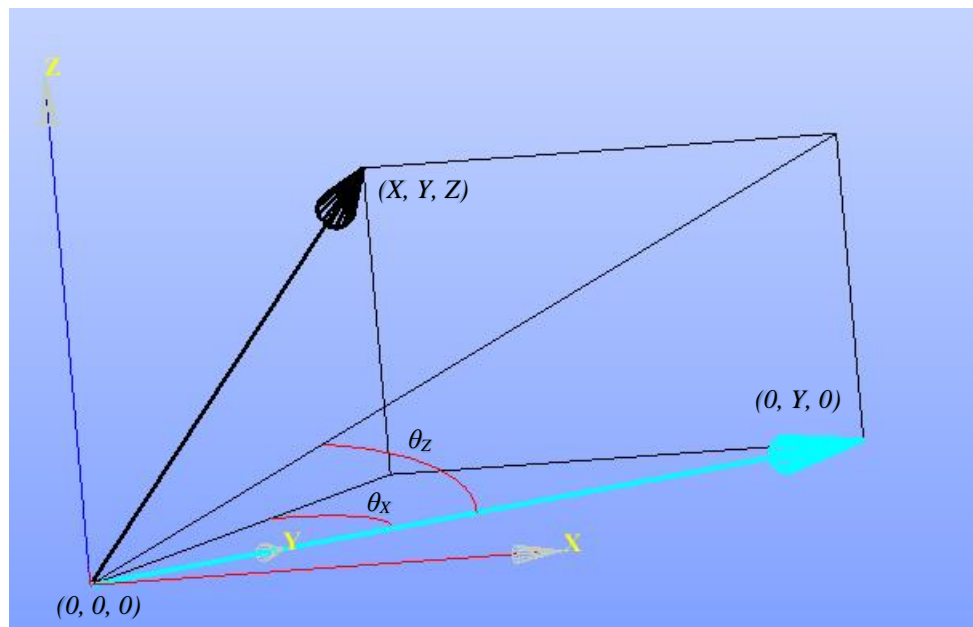


Figure 3-4 The AutoMoor coordinates used in the AM force calculations.

### Trelleborg DynaMoor and Port\_fairlead

A Trelleborg DynaMoor (DM) is a controllable moving hook on the berth connected to the end of a berth-vessel line. The application of DynaMoor is to maintain a minimum tension force of  $F_{min}$  and to cap the maximum line force at  $F_{max}$ . A schematic layout of a DynaMoor unit and its connection to the line and vessel is illustrated in Figure 3-4. In this

figure the DynaMoore unit is shown in green. A fixed berth-based fairlead leads the line connected to the DynaMoore. This fairlead is referred to as “Port\_fairlead”. In some designs the Port\_fairlead forms part of the DynaMoore unit, whereas in others it can be separated. Therefore, to make a generic model, two devices are defined, DynaMoore and Port\_fairlead.

The calculation of a force applied to the vessel due to a DynaMoore-connected line is the same as for a mooring line. One difference is that the berth connection point, used to calculate the line direction, is the Port\_fairlead instead of the berth-based bollard. The second difference is that the unstretched length of the line is not fixed in time. This is due to the pay-out/pay-in mechanism of the DynaMoore unit which holds the end of the line.

The unstretched length of the line is calculated based on the DynaMoore units’ hook position, at each time step. Whilst the line force is between  $F_{min}$  and  $F_{max}$ , the hook doesn’t move. However, if the line force falls below  $F_{min}$ , the hook moves away from Port\_fairlead (pay-in) and keeps the force at  $F_{min}$ . When the line force exceeds  $F_{max}$ , the hook moves toward the Port\_fairlead (pay-out) and keeps force at  $F_{max}$ . If the hook reaches any of the stop points ( $X_{min}$  or  $X_{max}$ ) then the force is the same as the line force, which can be smaller than  $F_{min}$  or larger than  $F_{max}$ .

The initial line tension,  $F_0$  is set to  $F_{min}$ , DynaMoore is located at  $X_0 = 0.0$  (considered to be mid-stroke of the unit), and elongation equivalent to  $F_0$  is looked up from the mooring line extension curve (MLEC)

$$E(\%) = MLEC(F_0), \tag{76}$$

At each time step the stretched length,  $L$ , and unstretched length,  $L_{un}$ , are calculated as follows

$$\begin{aligned} L &= L_{f_{pf}} + L_{f_w} + L_{D_{pf}} \\ (L_{un})_{old} &= L / (1.0 + \frac{E}{100}) \end{aligned} \tag{77}$$

Where,  $L_{f_w}$  is constant,  $L_{f_{pf}}$  is calculated based on the vessel position, and  $L_{D_{pf}}$  is controlled to satisfy the line force criterion. Then the line force criterion is checked to adjust the line’s unstretched length

$$\begin{aligned} &\left. \begin{array}{l} \text{if } F_{new} > F_{max}, F_{new} = F_{max} \\ \text{if } F_{new} < F_{min}, F_{new} = F_{min} \end{array} \right\} \text{ then } \left\{ \begin{array}{l} E(\%) = MLEC(F_{new}) \\ (L_{un})_{new} = L_{new} / (1.0 + \frac{E}{100}) \end{array} \right. \\ &\text{if } F_{min} < F_{new} < F_{max}, (L_{un})_{new} = (L_{un})_{old} \end{aligned} \tag{78}$$

And finally, the DynaMoore position is updated. The DynaMoore position is then checked to remain in the range  $[X_{min}, X_{max}]$ .

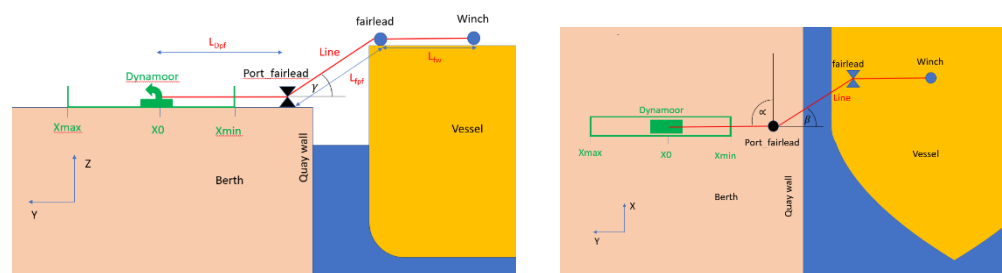


Figure 3-5 The DynaMoore layout: left) front view right) top view (not scaled).



The Port\_fairlead which leads the line, can be assembled to the DynaMoor device or it can be a separate device like a berth bollard. In either case, during operation the Port\_fairlead is fixed and doesn't move. So, all force calculations (vertical, horizontal, and total forces and line angle) are equivalent to a bollard but connected to two lines with the same force (Figure 3-6).

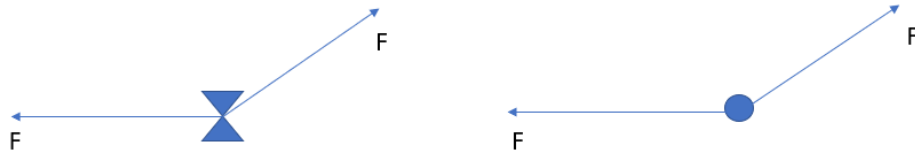


Figure 3-6 Forces applied to a Port\_fairlead forces: left) front view right) top view.

## Chains

The chain tension is derived using the catenary equation

$$H(t) \frac{d^2z}{dx^2} = -mg \sqrt{1 + \left(\frac{dz}{dx}\right)^2} \quad (79)$$

in which  $mg$  is the (submerged) chain weight,  $H(t)$  is the horizontal force of the chain at rest, and  $\frac{dz}{dx}$  is the local orientation of the chain element  $ds$  /6/.

The equation is solved for  $H$  using the Newton-Raphson method, in which  $H$  is used as initial estimate, which finally leads to  $F_{j,moor,chain}$ . In this method, it is considered that the maximum peak tension is

$$T_{max} = H + mgd \quad (80)$$

with the sag of the catenary  $d$ . It is further defined that the cable length

$$L_0 = \sqrt{\frac{2H}{mgd_0} + 1} \quad (81)$$

and the horizontal distance from the touch-down point to the surface point at rest is

$$x_0 = \frac{H}{mg} \cosh^{-1} \left( \frac{d_0 mg}{H} + 1 \right) \quad (82)$$

### 3.8.3 Wind forces

Wind forces are derived based on the OCIMF method /9/, in which

$$\begin{aligned}
 F_{x,w}(t) &= \frac{1}{2} C_{x,w} \rho_{air} V_w(t)^2 A_{T,w} \\
 F_{y,w}(t) &= \frac{1}{2} C_{y,w} \rho_{air} V_w(t)^2 A_{L,w} \\
 M_{xy,w}(t) &= \frac{1}{2} C_{xy,w} \rho_{air} V_w(t)^2 A_{L,w} L_{BP}
 \end{aligned} \tag{83}$$

with the density of air  $\rho_{air}$ , the transversal windage area  $A_{T,w}$ , the longitudinal windage area  $A_{L,w}$ , the length between perpendiculars  $L_{BP}$ , the wind speed  $V_w(t)$ . The wind drag coefficients  $C_{x,w}$ ,  $C_{y,w}$  and  $C_{xy,w}$  depend on the vessel type, the loading condition of the vessel and the angle of wind attack, e.g. see /3/ and /9/.

### 3.8.4 Current forces

Current forces are derived based on the OCIMF method /9/, in which

$$\begin{aligned}
 F_{x,c}(t) &= \frac{1}{2} C_{x,c} \rho_{water} V_c(t)^2 L_{BP} T \\
 F_{y,c}(t) &= \frac{1}{2} C_{y,c} \rho_{water} V_c(t)^2 L_{BP} T \\
 M_{xy,c}(t) &= \frac{1}{2} C_{xy,c} \rho_{water} V_c(t)^2 L_{BP} T
 \end{aligned} \tag{84}$$

with the density of water  $\rho_{water}$ , the transversal area affected by the current  $A_{T,c}$ , the longitudinal area affected by the current  $A_{L,c}$ , the length between perpendiculars  $L_{BP}$ , the current speed  $V_c$ . The areas affected by the current are determined from the vessel hull. The current drag coefficients  $C_{x,c}$ ,  $C_{y,c}$  and  $C_{xy,c}$  depend on the water depth to draft ratio of the vessel and the angle of current attack, e.g. see /9/. The OCIMF method uses a time series of current speed and direction.

However, this method cannot produce the drag-induced yaw moment under shear current flow conditions. Therefore, the panel method has been devised in order to calculate the current drag-induced yaw moment on the vessel for shear current. The input for this method is a two-dimensional (2D) current field consisting of the parameters water depth, and fluxes in  $x$  and  $y$  direction. The method involves

- Calculation of the current velocities in each element of the 2D flow field
- Interpolation of these velocities onto each panel
- Calculation of the average current speeds in  $x$  and  $y$  direction
- Calculation of the longitudinal and lateral drag force using the OCIMF method /9/.
- Projection of the current vectors onto the vessel grid panels
- Calculation of the force in each panel from the yaw moment using the drag equation (see equation (84)).

## 4 Numerical Implementation

In this section, the fundamental solution algorithms are given, and additional numerical aspects are commented. Figure 4-1 replicates the flow chart variables from Section 3, but additionally shows the distribution of the flow between the modules Frequency Response Calculator (FRC) and MIKE 21 Mooring Analysis (MA).

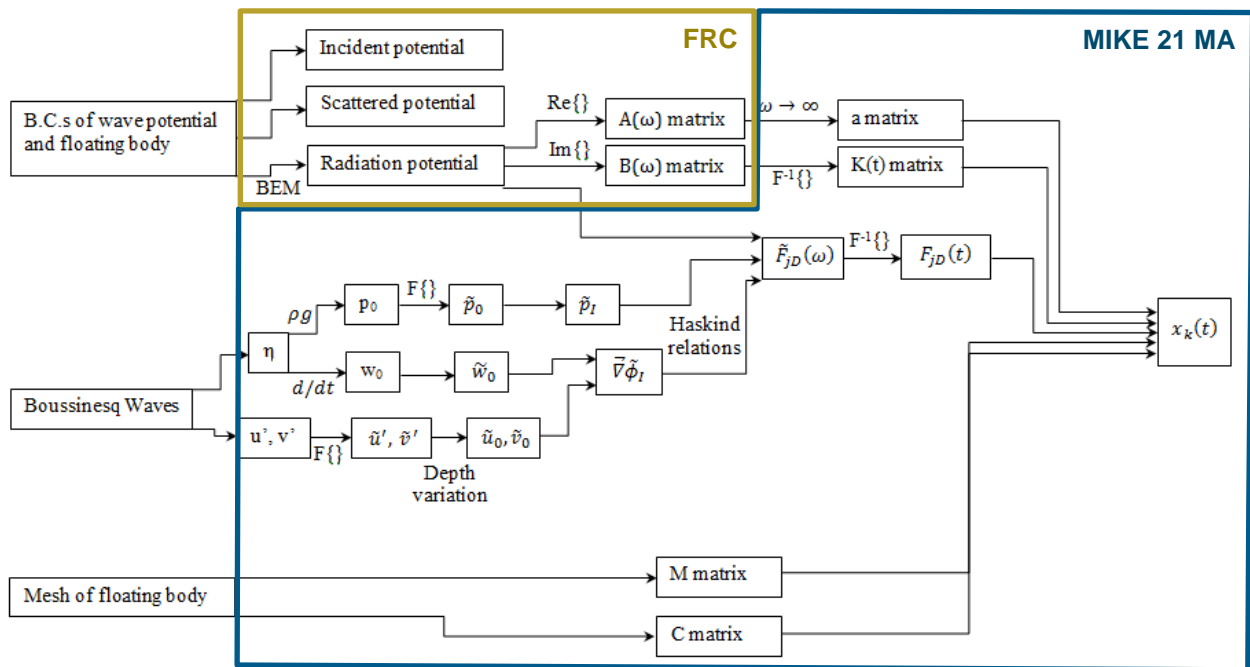


Figure 4-1 Flow chart of variables. The frames indicate the modules, dealing with the variables.

In Section 4.1, the implementation of the theory is provided. Section 4.2 outlines the treatment of the irregular frequencies, which can occur during the application of the boundary element method (BEM). Finally, the difference between Final computation mode and Convergence mode in MIKE 21 MA is explained.

### 4.1 Implementation of the theory

MIKE 21 MA solves the time-domain equations of motion (7) to obtain a time history of body motion in six degrees of freedom, due to a specified incident wave field, and mooring arrangement. This integration is performed using the explicit Runge-Kutta 4<sup>th</sup> order scheme, and a direct inversion of the inertia matrix.

The required hydrodynamic, hydrostatic and inertia coefficients of the body are computed using the low-order panel method program, FRC. FRC is used for performing a complete radiation analysis of the structure, that is  $A_{jk}(\omega)$ ,  $B_{jk}(\omega)$ , and  $\varphi_j(\omega)$  are computed at evenly-spaced frequencies over the entire significant domain of frequencies (including  $\omega = 0, \infty$ ).

We then use the fact that  $a_{jk} = A_{jk}(\infty)$ , and compute  $K_{jk}$  from the damping coefficients via equation (23). The inertia matrix,  $M_{jk}$ , and the hydrostatic matrix,  $C_{jk}$ , are direct output from FRC.

The incident wave exciting force,  $F_{jD}(t)$ , can be defined by providing the incident wave pressure and velocity at each panel centroid on the body (or these data can be computed by linearising the results of a MIKE 21 BW calculation over a rectangle of the free surface enclosing the body). In this case, the Haskind relations and the Fourier transform (51) are used for combining the incident wave data with the FRC radiation potentials to get the exciting forces. It can be shown that by using the complex conjugate of the radiation potentials in the Haskind relations, the correct forces are found. All Fourier transforms are done using the Fast Fourier Transformation (FFT).

Finally, instantaneous (non-linear) point forces on the structure due to each mooring line (or fender, or post) are computed based on the specified properties of the line/fender/post and the relative positions of the attachment points. These forces as well as the viscous damping forces proportional to a power of the body velocity, are all included at each sub-time step of the time integration.

## 4.2 Irregular frequencies

When a surface piercing body is analysed by boundary element techniques, numerical errors can occur at a number of irregular frequencies. In general, these irregular frequencies are higher than the frequency range of practical interest. DHI has implemented a technique, which first predicts the location of the irregular frequencies and smooth's the velocity potential around these frequencies using iterative smoothing techniques (see /12/). This method effectively minimises the irregular frequency effect, while still allowing for a fast run time.

The location of irregular frequencies can be calculated analytically for simple geometries. The analytical calculations for a rectangular prism can be extended through an equivalent box formulation to allow for the prediction of irregular frequencies  $\omega_{pm}$  in an arbitrarily-shaped 3D structure. This procedure is demonstrated in equation (4.1).

$$\begin{aligned}
 C_w &= \frac{A_w}{LOA * Beam}, C_m = \frac{A_m}{Beam * Draft}, C_c = \frac{A_c}{LOA * Draft} \\
 C_0 &= \frac{3}{4}, C_1 = \frac{1+6 * \frac{LOA-Beam}{LOA+Beam} * \ln p}{8}, C_2 = \frac{1+6 * \frac{LOA-Beam}{LOA+Beam} * \ln m}{8} \\
 B_0 &= C_w^{C_0}, B_1 = C_c^{C_1}, B_2 = C_m^{C_2} \\
 \alpha_1 &= \frac{LOA^2}{LOA^2+Beam^2}, \alpha_2 = \frac{Beam^2}{LOA^2+Beam^2} \\
 L_e &= B_1 * B_0^{\alpha_1}, B_e = B_2 * B_0^{\alpha_2}, h_e = \frac{\forall}{L_e * B_e} \\
 k_{pm} &= \pi * \sqrt{\left(\frac{p}{L_e}\right)^2 + \left(\frac{m}{B_e}\right)^2} \\
 \omega_{pm} &= \sqrt{g k_{pm} * \frac{1}{\tanh(k_{pm} h_e)}}
 \end{aligned} \tag{4.1}$$

where  $A_w$ ,  $A_m$  and  $A_c$  are the water plane, midsection and central longitudinal plane areas, and  $LOA$  is the length over all the vessel.  $p$  and  $m$  are indices from 1 to infinity, and  $k$  is the wave number.

## 4.3 Convergence mode

A simulation in convergence mode is a full simulation, in which usually no external forces are applied (although the user can apply long-term conditions such as river currents). Starting with an initial displacement of 0 in all six degrees of freedom, the simulation is repeated, until

1. the displacement at the end of the simulation does not exceed a threshold, given by the user OR
2. the maximum number of simulations (iterations) is reached.

The purpose of the convergence model is to achieve an equilibrium location of the vessel under the given mooring system prior to initiating the actual mooring simulation with e.g. wave forcing. When setting up the mooring system and pre-tensions, the system may not be perfectly balanced. This is ensured in the convergence model simulation.

## 5 Output Data

The output data of both Frequency Response Calculator (FRC) and MIKE 21 Mooring Analysis (MA) modules are summarised in this section.

### 5.1 Frequency Response Calculator

FRC provides the following results:

- Global output files
  - Vessel response file
  - Added mass coefficients
  - Damping coefficients
  - Drift forces
- Vessel specific output files
  - Response amplitude operator
  - Exciting forces

#### 5.1.1 Global output files

The vessel response file summarises all hydrostatic, gyrostatic and geometry data of the investigated floating body system such as

- Water depth
- Water density
- Vessel shape
- Vertical centre of gravity
- Draft radii of gyration
- Length over all
- Beam
- Maximum vessel height
- Submerged volume
- Added mass coefficients
- Damping coefficients
- Wave diffraction coefficients

The file is used as input for the subsequent calculations in MIKE 21 MA.

The added mass coefficients result file contains the added mass response for each degree of freedom as a function of wave frequency. The added mass is contained in a 6x6 matrix for each wave frequency and can be described as an inertia added to the system due to an acceleration of the vessel.

The damping coefficients result file contains the radiation damping of the vessel and is in the same format as the added mass. Radiation damping describes the energy lost in the vessel as it creates waves through motion.

The drift forces result file contains the second order drift surge and sway forces and yaw moments for each frequency and direction specified. This output file can only be generated if wave drift forces are included in the calculation.

## 5.1.2 Vessel-specific output files

The response amplitude operators result file contains the amplitude and phase data of the Response Amplitude Operator (RAO) for each frequency and direction specified. The RAO is a transfer function that can be used to determine the effect that a sea state will have upon the motion of a vessel.

The exciting forces result file contains the amplitude and phase data of the exciting forces and moments for each frequency and direction specified. The exciting force is the first order wave force on the vessel and is calculated using the Haskind relation (see Appendix A). The exciting force describes the combination of the incident wave forces from a harmonic wave and the diffraction force due to the vessel on the undisturbed wave field.

## 5.2 MIKE 21 MA

MIKE 21 MA provides the following results in both simulation modes:

- Global output files
  - Line positions
  - Line forces
  - Bollard forces
  - Fender forces
  - AutoMoor forces
  - AutoMoor displacements
  - DynaMoor forces
  - DynaMoor displacement
  - Port\_fairlead forces
  - Line pre-tension deviation (in convergence mode only)
- Vessel-specific output files
  - Vessel motion
  - Mooring force on vessel
  - External force
  - Surface elevation (in final computation mode only)
  - Chain forces

### 5.2.1 Global output files

The line forces result file contains an item for every specified mooring line, showing the dynamically-computed line force at each time step.

The line positions file contains the start and end-point of each mooring line for each time step. The information is sorted in three items: The x, y and z coordinate for each of the two points per line.

The bollard forces result file contains the horizontal bollard force components of all bollards included in the setup, followed by the vertical bollard force components and, finally, the total bollard forces. Data is provided for each time step.

The fender forces result file contains an item for every specified spatial fender, showing the dynamically-computed fender force as a function of time.

The AutoMoor forces result file contains 4 items for every specified spatial AutoMoor, showing the dynamically-computed AutoMoor forces at local x, y and z directions and total AM force as a function of time.

The AutoMoor displacements result file contains 6 items for every specified spatial AutoMoor, showing the dynamically-computed AutoMoor displacements of x and z, the Am length, vertical and horizontal angles (in x/y and z/y planes) as a function of time.

The DynaMoor forces result file contains 4 items for every specified spatial DynaMoor, showing the dynamically-computed DynaMoor forces at local x, y and z directions and total DynaMoor force as a function of time.

The DynaMoor displacements result file contains one item for every specified spatial DynaMoor, showing the dynamically-computed DynaMoors' displacements as a function of time.

The Port\_fairlead forces result file contains 4 items for every specified spatial Port\_fairlead, showing the dynamically-computed Port\_fairlead forces at local x, y and z directions and total Port\_fairlead force as a function of time.

In the convergence mode (see Section 4.3), the line pre-tension deviation is provided. It reflects the success of the convergence iteration process. This file contains an item for every specified spatial mooring line, and all these items will, at each iteration, contain data values representing the percentage deviation between the dynamically-computed line tension (at the iteration) and the line pre-tension. If a convergence is successful, then this file will at the last iteration step contain values, which are all smaller or equal the Line convergence threshold on the Convergence parameters dialog.

## 5.2.2 Vessel-specific output files

The vessel motion result file contains six items for the six degrees of freedom for each vessel, as a function of time. The definition of the items is provided in Figure 3-2.

The mooring force on vessel result file contains six items (three force items, three direction items) representing the force from mooring system on the vessel for each time step.

The external forces result file contains six items (three force items, three direction items) for each external forcing applied (wind, current, 2<sup>nd</sup> order drift forces), thus representing the force from each external forcing on the vessel for each time step.

The surface elevation result file contains the surface elevation at the vessels midpoint for each time step.

The diffraction force result file contains six items (three force items, three direction items) representing the diffraction force on the vessel for each time step.

The chain forces result file contains as many items as there are chains declared. The file displays the chain force evolution for each time step.



## 6 References

- /1/ Babarit, A., Delhommeau, G. (2015): "Theoretical and numerical aspects of the open source BEM solver NEMOH", LHEEA CNRS UMR 6598, Ecole Centrale de Nantes, France.
- /2/ Bingham, H.B. (2000): "A hybrid Boussinesq-panel method for predicting the motion of a moored ship", Coastal Engineering, 40, 21-38.
- /3/ Brix, J. (1993): "Manoeuvring Technical Manual", Seehafen Verlag, Hamburg, Germany.
- /4/ Delhommeau, G. (1987): "Les Problèmes de Diffraction-Radiation et de Résistance de Vagues: Etude Théorique et Résolution Numérique par la Méthode des Singularités", PhD thesis, Ecole Nationale Supérieure de Mécanique, Laboratoire d'Hydrodynamique Navale, Nantes, France.
- /5/ Delhommeau, G. (1993): "Seakeeping Codes AQUADYN and AQUAPLUS", In Proc. of the 19th WEGEMT School on Numerical Simulation of Hydrodynamics: Ships and Offshore Structures, Nantes, France.
- /6/ Irvine, H.M. (2000): "Cable Structures", MIT Press, Cambridge, MA, USA.
- /7/ Lighthill, J. (1979): "Waves and hydrodynamic loading", Proc. of the 2<sup>nd</sup> Int. Conf. on the Behaviour of Offshore Structures, BOSS '79, Vol. 1, 1-40.
- /8/ Newman, J.N. (1977): "Marine Hydrodynamics", MIT Press, Cambridge, Massachusetts, USA.
- /9/ Oil Companies International Marine Forum (2008): "Mooring Equipment Guidelines", 3<sup>rd</sup> edition, Witherby Seamanship International, Livingston, UK.
- /10/ Parisella, G., Gourlay, T.P. (2016): "Comparison of open-source code Nemoh with Wamit for cargo ship motions in shallow water", Research report 2016-23, Centre for Marine Science and Technology, Curtin University, October 2016, Perth, WA, Australia.
- /11/ Wehausen, J.V. and Laitone, E.V. (1960): "Surface Waves in Fluid Dynamics III", in Handbuch der Physik 9, Eds.: S. Flügge and C. Truesdell, pp 446-778, Springer Verlag.
- /12/ Zhu, X. and Lee, C.H. (1994): "Removing the Irregular Frequencies in Wave-Body Interactions", 9th International Workshop on Water Waves and Floating Bodies, Kizu, Japan.
- /13/ Delhommeau, G. (1993). "Numerical Simulation of Hydrodynamics: Ships and Offshore Structures". Nineteenth WEGMENT School.
- /14/ Newman, J.N. (1974). "Second-order Slowly-varying Forces on Vessels in Irregular Waves". In Int. Symposium on Dynamics of Marine Vehicles and Structures in waves.

### 6.1 Further reading on MIKE 21 MA and its predecessors

- Bhautoo, P. et. al. (2015): "Moored vessel interaction induced by passing ships at the Port of Brisbane", Australasian Coasts & Ports Conference, 15-18 September 2015, Auckland, New Zealand.

- Brüning, A. et. al. (2011): *“A hybrid modelling approach for floating breakwater dimensioning”*, 5th International Short Conference on Applied Coastal Research 2011.
- Brüning, A. et. al. (2014): *“Assessing mooring forces at an offshore wind terminal in Bremerhaven, Germany”*, PIANC World Congress, San Francisco, USA.
- Hansen, H.F. et al. (2009): *“Multi vessel interaction in shallow water”*, Proceedings of the 28th International Conference on Ocean, Offshore and Arctic Engineering OMAE2009, Honolulu, Hawaii, USA, May 31 - June 5, 2009.
- Hansen, H.F., Kirkegaard, J and Kofoed-Hansen, H. (2010): *“Hydraulic aspects of marine LNG receiving terminal design”*, Rio Oil & Gas Expo and Conference, Rio de Janeiro, September 13-16, 2010.
- Harkin, A., Mortensen, S. and Dixen, M. (2017): *“Validation of Moored Vessel Response Simulator with Physical Model Comparisons”*, Coasts & Ports 2017 Conference – Cairns, 21-23 June 2017.
- Jensen, B., Hansen, H.F. and Kirkegaard, J. (2015): *“Estimating Quadratic Transfer Functions for Floating Structures using Model Test Data from Irregular Sea States”*, Proceedings of the Twenty-fifth (2015) International Ocean and Polar Engineering Conference, Kona, Big Island, Hawaii, USA, June 21-26, 2015
- Kerper, D. et. al. (2017): *“Nearshore FSO Response under Rapidly Varying Landslide Tsunami Hydrodynamic Loads”*, Proceedings of the Twenty-seventh (2017) International Ocean and Polar Engineering Conference, San Francisco, CA, USA, June 25-30, 2017.
- Mortensen, S, Allery, C, Kirkegaard, J and Hancock, R, (2008): *“Numerical Modelling of Moored Vessel Motions Caused by Passing Vessels in the Port of Brisbane”*, Proceedings of the ASME 27th International Conference on Offshore Mechanics and Arctic Engineering OMAE 2008, June 15-20, 2008, Estoril, Portugal.
- Mortensen, S, Allery, C, Kirkegaard, J and Hancock, R. (2009): *“Numerical Modelling of Moored Vessel Motions Caused by Passing Vessels”*, Coast & Ports 2009 Conference Proceedings, Wellington, New Zealand.
- Stoschek, O, Leschka, S, Hein, C and Brüning, A. (2018): *“Optimizing Pier Structures using Dynamic Mooring Forces Modelling”*, PIANC-World Congress 2018, Panama City.

# APPENDIX A

## The Haskind Relation

## A The Haskind Relation

The Haskind relation is a way of finding the diffraction force without estimating the scattered potential. Instead, the force is found in a combination of the incoming wave field and the potential for the radiated wave field, which is the wave potential found for a moving body in a calm sea.

Expressed in a simplified way, the diffraction force is found by multiplying the radiated body movement on the incoming wave pressure field minus the radiation pressure field multiplied by the velocity of the incoming wave field. This seems quite abstract; therefore, the following heuristic explanation is given.

We have to go to structural engineering, where this principle is used extensively. In this field, the above statement can be found from the application of Betti's equation, also known as the reciprocity principle. In this case, a reduced form of the principle says

$$F^A u^B = F^B u^A \quad (\text{A.85})$$

In words, the equation says that for a system, a force from case A multiplied by the movement of case B is equal to the force from case B multiplied by the movement of case A. This equation is given without further proof; however, it is a well-established technique in structural engineering.

The diffraction force on the body can be written as the sum of a contribution from the incoming wave field and the scattered wave field:

$$F_D = F_I + F_S \quad (\text{A.86})$$

where  $F_D$  is the total diffraction force,  $F_I$  is the force due to the incoming wave field, and  $F_S$  is the force due to the scattered wave field. Note that  $F_I$  is also known as Froude-Krylov force. In the equation, there are two unknowns  $F_D$  that we want to find and  $F_S$  that has to be estimated. Let us say that the radiation potential is known and therefore also the force,  $F_R$ , using Betti's equation (A.85)

$$F_R u_S = F_S u_R \quad (\text{A.87})$$

In the above equation,  $u_S$  is apparently unknown, but at the body surface it can be related to the velocity found from the incoming wave,  $u_S = -u_I$ . Then, equation (A.86) is multiplied by  $u_R$ . Using equation (A.87) and substituting  $u_S$  with  $-u_I$ , gives the Haskind relation

$$F_D u_R = F_I u_R - F_R u_I \quad (\text{A.88})$$

This is basically the Haskind relation in a schematised form. The approach followed here is similar to the approach described in /7/, where it was used to find the second order force components. The derivation of the Haskind relations from conventional methods is given in /8/.